From photoelectron detachment spectra of BrHBr−, BrDBr− and IHI−, IDI− to vibrational bonding of BrMuBr and IMuI

Jörn Manz, Kazuma Sato, Toshiyuki Takayanagi, and Takahiko Yoshida

Citation: The Journal of Chemical Physics **142**, 164308 (2015); doi: 10.1063/1.4918980
View online: http://dx.doi.org/10.1063/1.4918980
View Table of Contents: http://scitation.aip.org/content/aip/journal/jcp/142/16?ver=pdfcov
Published by the AIP Publishing

From photoelectron detachment spectra of $BrHBr^-$, $BrDBr^-$ and IHI^-, IDI^- to vibrational bonding of BrMuBr and IMuI

Jörn Manz,[1,2] Kazuma Sato,[3] Toshiyuki Takayanagi,[3,a)] and Takahiko Yoshida[3]
[1]*State Key Laboratory of Quantum Optics and Quantum Optics Devices, Institute of Laser Spectrocopy, Shanxi University, Taiyuan 030006, China*
[2]*Freie Universität Berlin, Institut für Chemie und Biochemie, 14195 Berlin, Germany*
[3]*Department of Chemistry, Saitama University, Saitama City, Saitama 338-8570, Japan*

(Received 9 February 2015; accepted 14 April 2015; published online 28 April 2015)

Photoelectron detachment $XLX^-(00^00) + h\nu \rightarrow XLX(vib) + e^- + KER$ (X = Br or I, L = H or D) at sufficiently low temperatures photoionizes linear dihalogen anions XLX^- in the vibrational ground state ($v_1v_2^lv_3 = 00^00$) and prepares the neutral radicals XLX(vib) in vibrational states (vib). At the same time, part of the photon energy ($h\nu$) is converted into kinetic energy release (KER) of the electron [R. B. Metz, S. E. Bradforth, and D. M. Neumark, Adv. Chem. Phys. **81**, 1 (1992)]. The process may be described approximately in terms of a Franck-Condon type transfer of the vibrational wavefunction representing $XLX^-(00^00)$ from the domain close to the minimum of its potential energy surface (PES) to the domain close to the linear transition state of the PES of the neutral XLX. As a consequence, prominent peaks of the photoelectron detachment spectra (pds) correlate with the vibrational energies $E_{XLX,vib}$ of states XLX(vib) which are centered at linear transition state. The corresponding vibrational quantum numbers may be labeled vib = $(v_1v_2^lv_3) = (00^0v_3)$. Accordingly, the related most prominent peaks in the pds are labeled v_3. We construct a model PES which mimics the "true" PES in the domain of transition state such that it supports vibrational states with energies $E_{XLX,pds,00^0v_3}$ close to the peaks of the pds labeled v_3 = 0, 2, and 4. Subsequently, the same model PES is also used to calculate approximate values of the energies $E_{XMuX,00^00}$ of the isotopomers $XMuX(00^00)$. For the heavy isotopomers XHX and XDX, it turns out that all energies $E_{XLX,00^0v_3}$ are above the threshold for dissociation, which means that all heavy $XLX(00^0v_3)$ with wavefunctions centered at the transition state are unstable resonances with finite lifetimes. Turning the table, bound states of the heavy XLX are van der Waals (vdW) bonded. In contrast, the energies $E_{XMuX,00^00}$ of the light isotopomers $XMuX(00^00)$ are below the threshold for dissociation, with wavefunctions centered at the transition state. This means that $XMuX(00^00)$ are vibrationally bonded. This implies a fundamental change of the nature of chemical bonding, from vdW bonding of the heavy XHX, XDX to vibrational bonding of XMuX. For BrMuBr, the present results derived from experimental pds of $BrHBr^-$ and $BrDBr^-$ confirm the recent discovery of vibrational bonding based on quantum chemical *ab initio* calculations [D. G. Fleming, J. Manz, K. Sato, and T. Takayanagi, Angew. Chem., Int. Ed. **53**, 13706 (2014)]. The extension from BrLBr to ILI means the discovery of a new example of vibrational bonding. These empirical results for the vibrational bonding of IMuI, derived from the photoelectron spectra of IHI^- and IDI^-, are supported by *ab initio* simulations of the spectra and of the wavefunction representing vibrational bonding of IMuI. © *2015 AIP Publishing LLC.* [http://dx.doi.org/10.1063/1.4918980]

I. INTRODUCTION

The purpose of this paper is twofold: first, we show that experimental low resolution photoelectron detachment spectra (pds) of $BrHBr^-$ Refs. 1–3 and $BrDBr^-$ Refs. 1 and 2 allow to predict vibrational bonding of the light isotopomer BrMuBr, where Mu denotes muonium, the lightest isotope of hydrogen ($m_{Mu} = 1/9\, m_H$).[4,5] This conclusion shall be supported by corresponding analyses of *ab initio* quantum low and high resolution pds of $BrHBr^-$ and $BrDBr^-$. It is already known from the experimental spectra,[1–3] and also from complementary experimental[6,7] and quantum *ab initio*[8–10] investigations, that BrHBr and BrDBr are van der Waals (vdW) bonded. The present derivation of vibrational bonding of BrMuBr implies, therefore, a fundamental change in the nature of chemical bonding by isotopic substitution—this new isotope effect confirms the recent discovery of Ref. 10. The second purpose of this paper is to extend the analyses of experimental low resolution pds from $BrHBr^-$ and $BrDBr^-$ to IHI^- and IDI^-.[2,11] As a working hypothesis, this should predict the analogous change from vdW bonding of IHI and IDI[11] to vibrational bonding of IMuI.

Before starting, let us recall some important differences between vdW and vibrational bonding. In fact, they yield different structures, symmetries, and, most importantly, different energetics and mechanisms of chemical bonding of the

a)Author to whom correspondence should be addressed. Electronic mail: tako@mail.saitama-u.ac.jp

isotopomers, see Ref. 10 and also the pioneering quantum mechanical[12–19] and semiclassical[20,21] works on vibrational bonding. Thus, BrHBr and BrDBr are stabilized at the bottoms of one or the other vdW minima of their potential energy surface (PES), with corresponding symmetries $C_{\infty v}$ (linear structure) or C_s (bent), respectively. In contrast, the ground state of BrMuBr is stabilized at the linear transition state of the PES, with $D_{\infty h}$ symmetry. As a consequence, the PE increases when the vdW bonded BrHBr or BrDBr is dissociated into fragments Br + HBr or Br + DBr, from the vdW minima to the bottoms of the wells of the diatomic molecules HBr or DBr, in the asymptotic domains of the PES. At the same time, the vibrational zero point energies (ZPEs) decrease slightly from the values of the bound systems BrHBr or BrDBr to the fragments Br + HBr or Br + DBr. These roles of the PES and ZPE are reversed when the vibrationally bonded BrMuBr is dissociated into fragments Br + MuBr, which means the value of the PES decreases from the potential barrier to the asymptotic domain, but this is overcompensated by the even stronger increase of the vibrational ZPE. Turning the table, the fragments Br + MuBr are bonded to BrMuBr at the transition state due to the decrease of the vibrational ZPE which even over-compensates the increase in PES—this effect of the vibrational ZPE motivates the term "vibrational bonding."[12] Previous work on vibrational bonding already presented the mechanism, but tentative applications to BrHBr, BrDBr or IHI, IDI[12–21] suffered from inaccuracies of the assumed semi-empirical PESs with all-too-low barriers, which were falsified by the subsequent transition state spectroscopy experiments of Neumark and coworkers.[1–3,11] Hence, BrMuBr provides the first example of vibrational bonding, based on an accurate *ab initio* PES;[10] a new assessment of the accuracy of this PES will be based on the comparison of the experimental and theoretical pds, see Sec. III A. The present paper aims at confirmation of the first example, based on pds, and at the discovery of the second example, IMuI.

II. CONCEPTS AND METHODS

The way from experimental low resolution pds of the dihalogen hydride anions XHX^-, XDX^- to vibrational bonding of XMuX will be explained first for the example of the dibromine hydride, X = Br; analogous expressions apply to the diiodine hydride, X = I. To set the stage, we shall first summarize some important aspects of photoelectron detachment spectroscopy. Our presentation is based on the experimental publications by Neumark and coworkers,[1–3,11] and it also profits from their previous theoretical analyses,[22] but it is tailored to new quantum simulations on the level of standard vibrational Franck-Condon (FC) spectra $P_{XLX^-}(E)$ of XLX^-, (L = D or H), with the underlying assumptions adapted from Ref. 23, see also Refs. 24–26. In general, the corresponding anionic and neutral dihalogen hydrides and their fragments will be denoted as XLX^-, XLX and X^- + LX, X + LX, where L = D, H, or Mu.

Let us first consider some general aspects of photodetachment spectroscopy of XLX^- and the related transition state spectroscopy of XLX, see Figure 1. The PESs of XLX and XLX^- in their electronic ground states will be denoted by

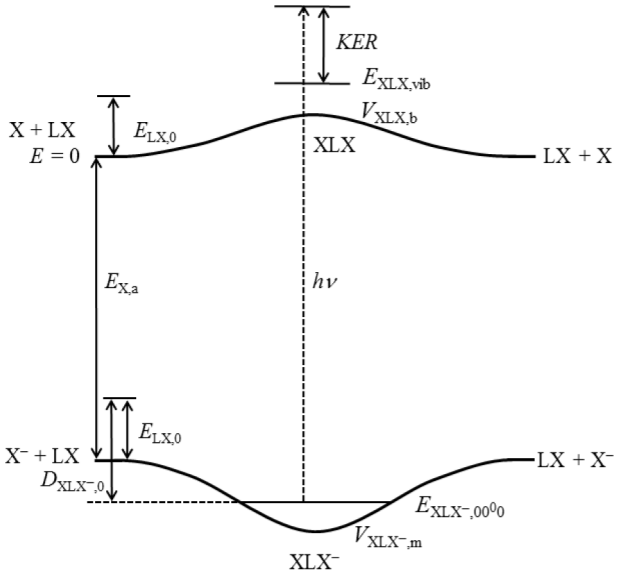

FIG. 1. Photodetachment spectroscopy of the XLX^- anion and the related transition state spectroscopy of the XLX radical (schematic).

V_{XLX} and V_{XLX^-}, respectively. Specifically, the highly accurate quantum chemical *ab initio* V_{BrLBr} for BrLBr is adapted from Ref. 10; for $BrLBr^-$, we employ the same level of *ab initio* quantum chemistry to determine V_{BrLBr^-}. In addition, we shall use the most prominent peaks of the pds of XLX^-,[1,2] in order to deduce the model $V_{XLX,pds}$ which serves as approximation of the accurate V_{XLX}, in the vicinity of its potential barrier. For convenience, the value of V_{XLX} in the asymptotic domain of the fragments X + LX, at the bottom of the well of the diatoms LX, is defined as zero energy, V_{XLX} (X + LX) = 0. The corresponding value of V_{XLX^-} in the asymptotic domain is V_{XLX^-} (X^- + LX) = $-E_{X,a}$, where $E_{X,a}$ is the electron affinity of the halogen atom X. The ground state energy of the diatomic molecule is termed $E_{LX,0}$. The value of V_{XLX} at its barrier is denoted as $V_{XLX,b}(>0)$. The potential minimum of V_{XLX^-} is called $V_{XLX^-,m}$. It turns out that the molecular structures of XLX^- at $V_{XLX^-,m}$ and of XLX at $V_{XLX,b}$ are close to each other, i.e., both have $D_{\infty h}$ symmetries with similar X–X distances (see Sec. III for further details).

Next, we consider the vibrational states of XLX^- and XLX which are supported by the PES V_{XLX^-} and V_{XLX}, or $V_{XLX,pds}$, respectively. The wavefunction $|\psi_{XLX^-,00^00}\rangle$ of the vibrational ground state of the anion XLX^- has energy $E_{XLX^-,00^00}$. Here, the quantum numbers $(v_1v_2^lv_3) = (00^00)$ express zero excitations of the symmetric stretch, the doubly degenerate bend, the pseudorotation, and asymmetric stretch, respectively. Accordingly, its zero point energy is $E_{XLX^-,00^00} - V_{XLX^-,m}$. It is evaluated as solution of the vibrational Schrödinger equation

$$H_{XLX^-}|\psi_{XLX^-,00^00}\rangle = E_{XLX^-,00^00}|\psi_{XLX^-,00^00}\rangle . \qquad (1)$$

The Hamiltonian H_{XLX^-} of XLX^- consists of two terms for the vibrational kinetic and potential energies, $H_{XHX^-} = T + V_{XLX^-}$. Likewise, the potential V_{XLX} of the neutral XLX supports vibrational states $|\psi_{XLX,vib}\rangle$ with energies $E_{XLX,vib}$, where "vib" denotes a set of vibrational quantum numbers (see below). These are evaluated as solutions of the vibrational

Schrödinger equation

$$H_{\mathrm{XLX}}\left|\psi_{\mathrm{XLX,vib}}\right\rangle = E_{\mathrm{XLX,vib}}\left|\psi_{\mathrm{XLX,vib}}\right\rangle, \tag{2}$$

with Hamiltonian $H_{\mathrm{XHX}} = T + V_{\mathrm{XLX}}$. Bound states of XLX have energies $E_{\mathrm{XLX,vib}}$ below the threshold $E_{\mathrm{LX},0}$; the others are vibrational resonance states or simply "resonances" with finite lifetimes. Neither Eq. (1) nor (2) considers any rotations and pseudorotations of XLX^- or XLX, respectively, in accord with the assumptions adapted from Ref. 23, compare with, e.g., Ref. 27. They are solved numerically as in Ref. 10, using cylindrical coordinates z, r, R, adapted from Ref. 22, which means R is the X–X internuclear distance, whereas z and r denote the projection and the distance of the nucleus of L on or from the interhalogenic axis, respectively. Using these coordinates, the kinetic energy operator is written as

$$T = -\frac{1}{2\mu_{XX}}\frac{\partial^2}{\partial R^2} - \frac{1}{2\mu}\left(\frac{\partial^2}{\partial r^2} + \frac{1}{r}\frac{\partial}{\partial r} + \frac{l^2}{r^2} + \frac{\partial^2}{\partial z^2}\right), \tag{3}$$

where the pseudo-rotation quantum number l associated with the ϕ coordinate motion is taken to be zero (see Figure 2). The values of z, r, R at the barrier of V_{XLX} are equal to 0, 0, $R_{\mathrm{XLX,b}}$, respectively.

The density $\rho_{\mathrm{XLX^-},00^00}(z,r,R) = \left|\left\langle z,r,R|\psi_{\mathrm{XLX^-},00^00}\right\rangle\right|^2$ of XLX^- in the vibrational ground state is centered at the potential minimum $V_{\mathrm{XLX^-,m}}$, where z, r, $R = 0$, 0, $R_{\mathrm{XLX^-,m}}$. The photoelectron detachment spectra are dominated by transitions from XLX^- to XLX which start in the ground state 00^00 of the precursor anion.[2] Accordingly, the energetic threshold for dissociation $XLX^- \rightarrow X^- + XL$ is equal to the corresponding gap between the levels of the vibrational ground states of XLX^- and its fragments $X^- + LX$,

$$D_{\mathrm{XLX^-},0} = -E_{\mathrm{X,a}} + E_{\mathrm{LX},0} - E_{\mathrm{XLX^-},00^00}. \tag{4}$$

Next, let us consider some additional energetic aspects of photoelectron detachment spectroscopy, see Figure 1. The precursor anions XLX^- are photodetached, $XLX^- \rightarrow XLX + e^-$, by means of photons with energies $h\nu$. This way, the neutrals XLX may be generated in the vibrational states $|\psi_{\mathrm{XLX,vib}}\rangle$ with energies $E_{\mathrm{XLX,vib}}$. The supplementary energy KER is released (R) and monitored as kinetic energy (KE) of the photodetached electron. The energy balance is thus

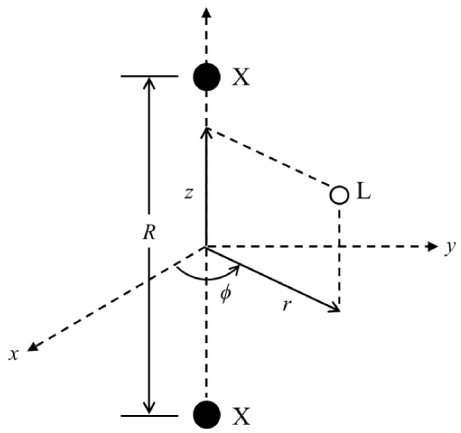

FIG. 2. Cylindrical coordinates used in this study.

$$h\nu = E_{\mathrm{XLX,vib}} - E_{\mathrm{XLX^-},00^00} + \mathrm{KER} \tag{5a}$$

$$= D_{\mathrm{XLX^-},0} + E_{\mathrm{XLX,vib}} - E_{\mathrm{LX},0} + E_{\mathrm{X,a}} + \mathrm{KER}. \tag{5b}$$

Traditionally, the photoelectron detachment spectra are plotted versus KER, for fixed value of $h\nu$.[1–3,11] For the given values of $h\nu$, $D_{\mathrm{XLX^-},0}$, $E_{\mathrm{X,a}}$, and $E_{\mathrm{LX},0}$, spectral peaks at specific values of KER then allow to determine the energies $E_{\mathrm{XLX,vib}}$ of selected vibrational states $|\psi_{\mathrm{XLX,vib}}\rangle$ of XLX which are prepared by photodetachment. Below, we shall employ an equivalent way of drawing the spectra versus energy,

$$E = h\nu - \mathrm{KER} - D_{\mathrm{XLX^-},0} - E_{\mathrm{X,a}} + E_{\mathrm{LX},0}, \tag{6}$$

with corresponding peaks at energies $E = E_{\mathrm{XLX,vib}}$ of the selected states $|\psi_{\mathrm{XLX,vib}}\rangle$.

Now, we turn to the quantum simulations of the pds of XLX^- (in arbitrary units of intensities). Following Ref. 23 and using Eq. (6),

$$P_{\mathrm{XLX^-}}(E) = \frac{1}{\pi\hbar}Re\int_0^\infty dt\,\exp(iEt/\hbar)C(t) \times \exp(-t^2/2\tau_{\mathrm{XLX}}^2) \tag{7a}$$

$$= \frac{1}{\pi\hbar}\sum\nolimits_{\mathrm{vib}}\left|\left\langle\psi_{\mathrm{XLX^-},00^00}|\psi_{\mathrm{XLX,vib}}\right\rangle\right|^2 Re \times \int_0^\infty dt\,\exp(i(E - E_{\mathrm{XLX,vib}})t/\hbar) \times \exp(-t^2/2\tau_{\mathrm{XLX}}^2) \tag{7b}$$

$$= \frac{1}{\pi\hbar}\sum\nolimits_{\mathrm{vib}}\left|\left\langle\psi_{\mathrm{XLX^-},00^00}|\psi_{\mathrm{XLX,vib}}\right\rangle\right|^2 \times \exp(-(E - E_{\mathrm{XLX,vib}})^2/2\Delta E_{\mathrm{XLX}}^2) \tag{7c}$$

$$= \left\langle\psi_{\mathrm{XLX^-},00^00}|\psi_{\mathrm{XLX^-},0}(E;\tau_{\mathrm{XLX}})\right\rangle. \tag{7d}$$

The autocorrelation function

$$C(t) = \left\langle\psi_{\mathrm{XLX^-},00^00}|\psi_{\mathrm{XLX^-},00^00}(t)\right\rangle \tag{8a}$$

$$= \left\langle\psi_{\mathrm{XLX^-},00^00}|\exp(-iH_{\mathrm{XLX}}t/\hbar)\psi_{\mathrm{XLX^-},00^00}\right\rangle \tag{8b}$$

in Eq. (7a) is evaluated by propagating the wavefunction $|\psi_{\mathrm{XLX^-},00^00}\rangle$ of the ground state of the anion XLX^- on the PES of the neutral XLX, by means of the split operator technique.[28] The empirical Gaussian damping function $\exp(-t^2/2\tau_{\mathrm{XLX}}^2)$ accounts for homogeneous effects of dissociative or radiative resonance decay, as well as for inhomogeneous effects, including vibrational-rotational and pseudorotational couplings that could not be monitored in the spectra, but which contribute to their low resolutions.[1–3,11] Equation (7b) is adapted from the pioneering Ref. 24. Equation (7c) shows that the time dependent representation (Eq. (7)) is equivalent to a sum of Gaussians $\left|\left\langle\psi_{\mathrm{XLX^-},00^00}|\psi_{\mathrm{XLX,vib}}\right\rangle\right|^2\exp(-(E - E_{\mathrm{XLX,vib}})^2/2\Delta E_{\mathrm{XLX}}^2)$ which are centered at the vibrational energies $E_{\mathrm{XLX,vib}}$ of XLX. The width parameters ΔE_{XLX} are reciprocal to τ_{XLX},

$$\Delta E_{\mathrm{XLX}} = \hbar/\tau_{\mathrm{XLX}}. \tag{9}$$

Accordingly, quantum simulations of low (large ΔE_{XLX}) and high (small ΔE_{XLX}) resolution pds depend on small and large values of τ_{XLX}, respectively. We employ the same values $\tau_{\mathrm{XLX}} = \tau_{\mathrm{XHX}} = \tau_{\mathrm{XDX}}$ (or equivalently $\Delta E_{\mathrm{XLX}} = \Delta E_{\mathrm{XHX}} = \Delta E_{\mathrm{XDX}}$) for the two isotopomers XHX and XDX: this and the electron affinity $E_{\mathrm{X,a}}$ are the only empirical parameters which are used in our simulations of the spectra.[1,2]

Equation (7d) relates the spectrum to the energy (E)- and τ_{XLX}-dependent scattering wavefunction,[23]

$$\begin{aligned}&|\psi_{XLX^-,00^00}(E;\tau_{XLX})\rangle\\&\quad=\frac{1}{\hbar}Re\int_{-\infty}^{\infty}dt\exp(iEt/\hbar)\,|\psi_{XLX^-,00^00}(t)\rangle\\&\qquad\times\exp(-t^2/2\tau_{XLX}^2).\end{aligned}\tag{10}$$

In the ideal case where $E = E_{XLX,vib}$ and $\tau_{XLX} \to \infty$, scattering wavefunction (10) approaches the vibrational wavefunction,[23,24]

$$|\psi_{XLX^-,00^00}(E = E_{XLX,vib};\tau_{XLX}\to\infty)\rangle \to |\psi_{XLX,vib}\rangle\,.\tag{11}$$

Finally, we develop the strategy that should allow us to employ the experimental pds of XDX^- and XHX^-, in order to deduce vibrational bonding of XMuX. For this purpose, we make use of the decomposition of $P_{XLX^-}(E)$ into a sum of Gaussians with amplitudes that are proportional to the squares of the vibrational FC factors $\langle\psi_{XLX^-,00^00}|\psi_{XLX,vib}\rangle$ for the ground state $|\psi_{XLX^-,00^00}\rangle$ of the anion XLX^-, projected on the vibrational state $|\psi_{XLX,vib}\rangle$ of the neutral XLX, cf. Eq. (7c). Obviously, pronounced peaks in the experimental spectra, or in the simulated ones, point to vibrational states $|\psi_{XLX,vib}\rangle$ of the neutral XLX which have large FC factors, which means they are similar to the ground state $|\psi_{XLX^-,00^00}\rangle$ of the anion XLX^-. Since $|\psi_{XLX^-,00^00}\rangle$ is centered at the potential minimum $V_{XLX^-,m}$ of XLX^- and, furthermore, since the geometric structures of XLX^- at $V_{XLX^-,m}$ are close to that of XLX at $V_{XLX,b}$ (*vide infra*), we conclude that the peaks of the photodetachment spectra are close to the energies $E_{XLX,vib}$ of vibrational states of XLX which are represented by wavefunctions $|\psi_{XLX,vib}\rangle$ that are centered at the barrier of the PES of the neutral XLX. If the corresponding state is a bound state, i.e., if $E_{XLX,vib} < E_{XL,0}$, then this is a vibrationally bonded state. Else, it is a vibrational resonance with "character of vibrational bonding," because it is localized close to the potential barrier $V_{XLX,b}$. For a simple derivation of vibrational bonding in XMuX from photoelectron detachment spectra of XDX^- and XHX^-, it suffices, therefore, to focus on their spectral peaks—these should be close to the energies $E_{XLX,vib}$ of the corresponding vibrational bonded states, or to the resonances with "character of vibrational bonding." In order to reproduce the energies $E_{XLX,vib}$ at the peaks of the spectra, it is, however, not necessary to solve vibrational Schrödinger Eq. (2) with the global V_{XLX} that accounts for all domains that might ever be visited by XLX. Instead, one may restrict V_{XLX} to the domain of the potential barrier or, even simpler, employ a parametrized model potential $V_{XLX,pds}$ which resembles V_{XLX} in the domain of the barrier; its parameters may then be determined such that the modified vibrational Schrödinger equation

$$H_{XLX,pds}\,|\psi_{XLX,pds,vib}\rangle = E_{XLX,pds,vib}\,|\psi_{XLX,pds,vib}\rangle\tag{12}$$

with Hamiltonian $H_{XLX,pds} = T + V_{XLX,pds}$ (instead of $H_{XLX} = T + V_{XLX}$) yields vibrational states supported by $V_{XLX,pds}$ with energies $E_{XLX,pds,vib}$ close to the most prominent peaks of the experimental spectra $P_{XLX^-}(E)$, L = H or D. Equation (12) with the same empirical $V_{XLX,pds}$ may then be used to calculate the approximate zero point energy $E_{XMuX,pds,0}$ of XMuX. If $E_{XMuX,pds,0}$ satisfies the criterion $E_{XMuX,pds,0} < E_{MuX,0}$, then we can predict that XMuX is vibrationally bonded, with its vibrational wavefunction centered at the potential barrier.

The parametrized three-dimensional (3D) model potential $V_{XLX,pds}$ should reproduce the most important characteristics of the "true" potential V_{XLX} at its barrier. In particular, the three 1D profiles along z and r, R across the barrier should have double and single minima, respectively.[10,22] We have tested various parametrized 3D model potentials $V_{XLX,pds}$ which satisfy these criteria, including not only harmonic but also higher order polynomial or double Morse potentials,[29] and all gave similar results, which means all the conclusions are robust with respect to the choice of the form of the empirical potential. Exemplarily, we shall present the results obtained by means of the model potential which consists of a sum of contributions for the symmetric stretch (v_1) along R, the doubly degenerate bend (v_2) along r (without any pseudorotations, $l = 0$), and the antisymmetric stretch (v_3) along z,

$$\begin{aligned}V_{XLX,pds}(z,r,R) = {}& V_{XLX,pds,b} + V_{R,XLX}(R;f_{R,XLX},R_{XLX,b})\\&+V_{r,XLX}(r;f_{R,XLX})\\&+V_{z,XLX}(z;f_{z,XLX},z_{e,XLX},V_{lr,XLX}),\end{aligned}\tag{13}$$

with barrier height $V_{XLX,pds,b}$ and harmonic potentials

$$V_{R,XLX}(R;f_{R,XLX},R_{XLX,b}) = \frac{1}{2}f_{R,XLX}(R-R_{XLX,b})^2,\tag{14}$$

$$V_{r,XLX}(r;f_{r,XLX}) = f_{r,XLX}r^2\tag{15}$$

for the symmetric stretch and doubly degenerate bends; the corresponding harmonic frequencies are denoted by $\omega_{1,XLX}$ and $\omega_{2,XLX}$, respectively. The double well potential $V_{z,XLX}(z;f_{z,XLX},z_{e,XLX},V_{lr,XLX})$ for the antisymmetric stretch is constructed as lower adiabatic potential that corresponds to two "left" (l) and "right" (r) diabatic harmonic potentials with force constant $f_{z,XLX}$, coupling $V_{lr,XLX}$, and minima at $-z_{e,XLX}$ and $+z_{e,XLX}$, respectively,

$$\begin{aligned}&V_{z,XLX}(z;f_{z,XLX},z_{e,XLX},V_{lr,XLX})\\&\quad=\frac{1}{2}f_{z,XLX}z^2+V_{lr}+((f_{z,XLX}\cdot z\cdot z_{e,XLX})^2\\&\qquad+V_{lr,XLX}/4)^{1/2}.\end{aligned}\tag{16}$$

From the analyses of Refs. 1–3, 11, and 22, it is known that the sequence of the three lowest, most prominent peaks in the experimental spectra correlates with excitations of the antisymmetric stretch, $v_3 = 0$, 2, and 4. Vibrational states with odd quantum numbers $v_3 = 1,3,\ldots$ are not excited, for symmetry reasons. The set of vibrational quantum numbers of the states which correlate with the most prominent spectral peaks is thus assumed to be vib = (00^0v_3), and for simplicity, the peaks are labeled by v_3. Inserting model potential Eqs. (13)–(16) then yields the approximate energies

$$\begin{aligned}E_{XLX,pds,00^0v_3} = {}& V_{XLX,pds,b}+\frac{1}{2}\hbar\omega_{1,XLX}\\&+\hbar\omega_{2,XLX}+E_{XLX,pds,v_3},\end{aligned}\tag{17}$$

where E_{XLX,pds,v_3} is evaluated as solution of the 1D Schrödinger equation for the antisymmetric stretch with model potential $V_{z,XLX}(z;f_{z,XLX},z_{e,XLX},V_{lr,XLX})$. By construction, the corresponding wavefunctions are centered at or close to the potential barrier. Hence, they represent either vibrationally bonded

states or resonances with "character of vibrational bonding" if $E_{XLX,pds,00^0v_3} < E_{LX,0}$ or $> E_{LX,0}$, respectively. The frequency $\omega_{1,XLX}$ of the symmetric stretch is the same for all isotopomers XHX, XDX, and XMuX; hence, one may employ the parameter $V_{XLX,pds,B} = V_{XLX,pds,b} + 0.5\hbar\omega_{1,XLX}$, where the contribution of the symmetric stretch turns out to be negligible, see Sec. III. Energies (17) depend, therefore, on altogether five parameters ($V_{XLX,pds,B}$, $f_{r,XLX}$, $f_{z,XLX}$, $z_{e,XLX}$, and $V_{rl,XLX}$) of model potential (13)–(16). The values of these five parameters are determined by means of a genetic algorithm[30] such that they yield good agreement of energies (17) with the peaks labeled $v_3 = 0$, 2, and 4 of the experimental photodetachment spectra of the two isotopomers XHX^- and XDX^-, respectively. The genetic algorithm uses the energies of these altogether six peaks of the experimental photoelectron detachment spectra as input, exclusively.

III. RESULTS AND DISCUSSIONS

A. From photoelectron detachment spectra of $BrHBr^-$ and $BrDBr^-$ to vibrational bonding of BrMuBr

The experimental low resolution photoelectron detachment spectra of $BrHBr^-$ and $BrDBr^-$ Refs. 1 and 2 are compared with the present quantum simulations in Figures 3(a) and 4(a), respectively. The energetic domain $0.0 < E < 0.6$ eV is chosen such that the nascent BrLBr radicals are generated exclusively in the electronic ground state.[1,2,22] The theoretical low and high resolution spectra are simulated using time-dependent approach (7)–(9) ($0 < t < 200\,000\hbar/E_h \sim 4.8$ ps), with damping parameters τ_{BrLBr} (or with equivalent parameters for the energy resolution ΔE_{BrLBr}, cf. Eq. (9)) as specified in the caption of Figure 3. For the balance of energy, Eq. (6), we employ the experimental value of the photon energy, $h\nu = 5.825$ eV,[1,2] together with the value of the electron affinity $E_{Br,a} = 3.365$ eV adapted from Ref. 31, and the vibrational zero point energies $E_{HBr,0} = 0.163$ eV and $E_{DBr,0} = 0.117$ eV. The latter are calculated using the *ab initio* PES V_{BrLBr} adapted from Ref. 10, in gratifying agreement with the values 0.163 eV and 0.116 eV from the NIST database.[32] Moreover, we use new quantum *ab initio* values $D_{BrHBr^-,0} = 0.958$ eV and $D_{BrDBr^-,0} = 0.953$ eV; gratifyingly, these are within the error bars of the previous experimental result, $D_{BrLBr^-,0} = 0.91 \pm 0.05$ eV.[33]

Figures 3(a) and 4(a) also compare the values of the experimental (in brackets) and theoretical (without brackets) energies of the peaks labeled $v_3 = 0$, 2, and 4, in the domain $E < 0.6$ eV. This comparison allows a new assessment of the accuracy of the *ab initio* potential V_{BrLBr},[10] beyond the previous value ±0.017 eV of its uncertainty for energies <0 eV, based on the comparison of the values of its van der Waals minima and those of Ref. 9. For the new, relevant extended domain $0 < E < 0.6$ eV, the maximum value of the deviations between the experimental and theoretical spectral peaks is 0.046 eV. This tells us that the energy levels derived from our PES may have inaccuracy of ±0.046 eV. Fortunately, this uncertainty is below the binding energy 0.056 eV of BrMuBr, confirming vibrational bonding of BrMuBr.[10] In addition to the deviations between the present theoretical pds and the experimental ones adapted from Ref. 2, comparison of the results of Refs. 1–3 suggests that the experimental peak energies should be considered within some boundaries $\pm\Delta E(v_3)$, which increase from ±0.025 eV to ±0.035 eV as v_3 increases from 0 to 4. This is in accord with the energetic width parameter $\Delta E_{BrLBr} = 0.029$ eV which is used for the present simulation of the low resolution pds, cf. the caption of Figure 3. Accordingly, the agreement of the selected theoretical and experimental[1,2] peak energies of the photoelectron detachment spectra is satisfactory, in particular, since our *ab initio* simulations are supplemented by just two parameters, the electron affinity $E_{Br,a}$ and the energy resolution Δ_{BrLBr}, see Eqs. (4) and (9). The fits of the photoelectron detachment spectra which are presented in Ref. 2 appear even better, but they are based on empirical potentials with several additional parameters—needless to add, the larger the number of the parameters, the better are the fits of the spectra. In any case, all peak energies are above the values of the thresholds $E_{LBr,0}$ [in square brackets], which means they correlate with resonances that have dominant character of vibrational bonding, not with vibrationally bonded states, in accord with the conclusions drawn by the experimentalists.[1,2,22]

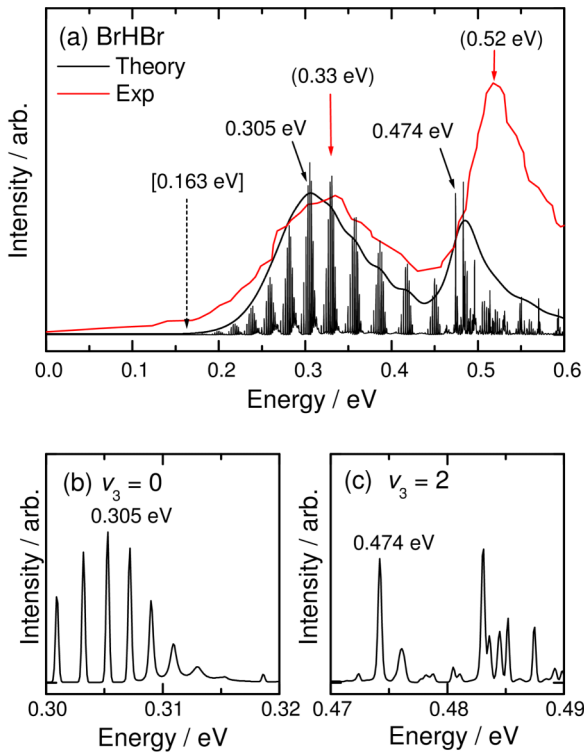

FIG. 3. (a) Comparison of the experimental low resolution photoelectron photodetachment spectrum of $BrHBr^-$ (adapted from Refs. 1 and 2) with the present theoretical low and high resolution spectra. The latter are simulated using Eqs. (5)–(7) with parameters $\tau_{BrLBr} = 1.6\times10^3\hbar/E_h$ and $1.6\times10^5\hbar/E_h$, corresponding to the parameters for energy resolution, $\Delta E = 29$ meV and 0.29 meV, respectively. The energies of the experimental peaks (in brackets) in the domain $0.0 \text{ eV} < E < 0.6$ eV are compared with the theoretical levels $E_{BrHBr,vib}$ (without brackets) for the vibrational quantum numbers $vib = (v_1 v_2^l v_3) = (00^0 v_3)$, $v_3 = 0$, 2, 4. Panels (b) and (c) show blow-ups of the theoretical high resolution spectra in the energetic vicinities of the peaks labeled $v_3 = 0$ and 2, respectively. The dashed vertical arrow indicates the threshold $E_{HBr,0}$ [in square brackets] between the levels of (van der Waals) bound states ($<E_{HBr,0}$) and resonances with finite lifetimes ($>E_{HBr,0}$).

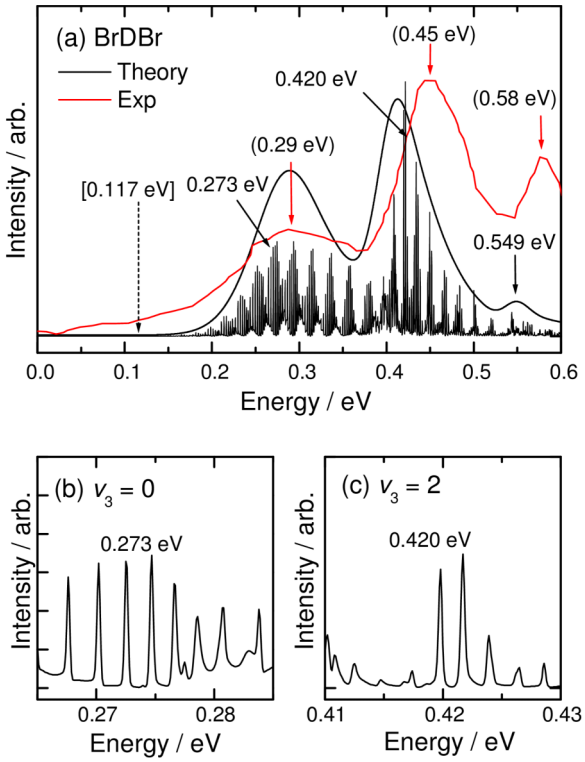

FIG. 4. Comparison of the experimental low resolution photoelectron photodetachment spectrum of $BrDBr^-$ (adapted from Refs. 1 and 2) with the present theoretical low and high resolution spectra. The notations are analogous to those of Figure 3.

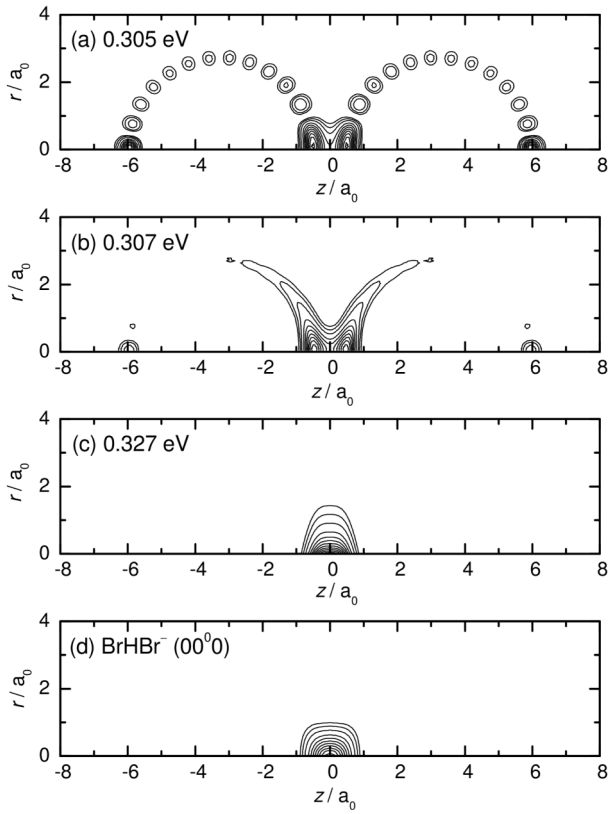

FIG. 5. (a) 2D equidensity plot of the 3D wavefunction $\langle z, r, R|\psi_{\mathrm{BrHBr,vib}}\rangle$ of BrHBr at internuclear Br-Br distance $R = 6.5\,a_0$, with quantum numbers vib $= (v_1 = 0, v_2{}^l = 0^0, v_3 = 0)$ and energy $E_{\mathrm{BrHBr,vib}} = 0.305$ eV at the first peak ($v_3 = 0$) of the pds shown in Figures 3(a) and 3(b). The coordinates r and z specify the distance and the projection of the proton from or on the internuclear Br-Br axis; corresponding 3D equidensity contours may be generated by rotating the 2D contours around this axis, which coincides with z. The wavefunction is evaluated as scattering wavefunction $\langle z, r, R|\psi_{\mathrm{BrHBr},00^00}; E, \tau_{\mathrm{XLX}})\rangle$ using Eq. (10) with energy $E = 0.305$ eV and damping parameter $\tau_{\mathrm{BrLBr}} = 1.6\times10^5\hbar/E_{\mathrm{h}}$ (or $\Delta E = 0.29$ meV) for high resolution pds. (b) Same as (a), but using the damping parameter $\tau_{\mathrm{BrHBr}} = 1.6\times10^3$ meV (or $\Delta E = 29$ meV) for simulation of the low resolution pds. The mean energy 0.307 eV of this scattering wavefunction is close to $E = E_{\mathrm{BrHBr,vib}} = 0.305$ eV, in accord with Eq. (11). (c) 2D equidensity plot of the 3D wavefunction $\langle z, r, R|\psi_{\mathrm{BrHBr,vib,pds}}\rangle$ (at internuclear Br-Br distance $R = 6.5\,a_0$) with quantum numbers vib $= (00^00)$ and energy $E_{\mathrm{BrHBr,vib,pds}} = 0.327$ eV. It is evaluated using Eq. (10) with model potential (13)–(16) and with parameters derived from the peaks of the experimental pds, which means $\langle z, r, R|\psi_{\mathrm{BrHBr,vib,pds}}\rangle$ is an approximation to $\langle z, r, R|\psi_{\mathrm{BrHBr,vib}}\rangle$, in the vicinity of the potential barrier. Likewise, its energy $E_{\mathrm{BrHBr,vib,pds}} = 0.327$ eV is an approximation to $E_{\mathrm{BrHBr,vib}} = 0.305$ eV. (d) 2D equidensity plot of the 3D wavefunction $\langle z, r, R|\psi_{\mathrm{BrHBr^-},00^00})\rangle$ of the ground state of $BrHBr^-$, at internuclear Br–Br distance $R = 6.5\,a_0$.

Blow-ups of the theoretical high resolution pds of $BrHBr^-$ and $BrDBr^-$ in the vicinity of the peaks labeled $v_3 = 0$ and 2 are shown in Figures 3(b) and 3(c) and Figures 4(b) and 4(c), respectively. The selection of the peak in the high resolution spectra which correlates with the resonance that has the "best" character of vibrational bonding depends on the corresponding resonance wavefunction. The criterion is that its density should be centered at the potential barrier, as much as possible. The resulting "best" peaks turn out to be neighbours of the highest spectral peaks, always; they are populated by means of slightly non-vertical FC excitations, essentially from the minimum of the PES of the anion at $R_{\mathrm{BrLBr^-,m}} = 6.42\,a_0$ to the barrier of the PES of the neutral at $R_{\mathrm{BrLBr,b}} = 6.16\,a_0$.

It is instructive to consider the selective 3D resonance wavefunctions with "best" character of vibrational bonding and with energies $E_{\mathrm{BrLBr,vib}}$ close to the peaks of the photodetachment spectra in some detail. Exemplarily, the wavefunction $\langle z, r, R|\psi_{\mathrm{BrHBr,vib}}\rangle$ of BrHBr with quantum numbers vib $= (v_1 v_2{}^l v_3) = (00^00)$ which is associated with the peak labeled $v_3 = 0$ ($E_{\mathrm{BrHBr,vib}} = 0.305$ eV in Figure 3(b)) is illustrated in Figure 5(a), by means of two-dimensional (2D) equidensity contours. It is evaluated as scattering wavefunction $\langle z, r, R|\psi_{\mathrm{XLX^-},00^00}(E; \tau_{\mathrm{XLX}})\rangle$ using Eq. (10) with resonance energy $E = 0.305$ eV and with damping parameter $\tau_{\mathrm{BrLBr}} = 1.6\times10^5\hbar/E_{\mathrm{h}}$, corresponding to the parameter for high energy resolution, $\Delta E = 0.29$ meV. The equidensity contours are robust with respect to even larger values of τ_{BrLBr}, in accord with convergence to limit (11), which means Figure 5(a) documents an eigen-(resonance)-state of BrHBr. The corresponding scattering function $\langle z, r, R|\psi_{\mathrm{BrHBr^-},0}(E; \tau_{\mathrm{BrHBr}})\rangle$ for the low resolution pds ($\tau_{\mathrm{BrHBr}} = 1.6\times10^3\hbar/E_{\mathrm{h}}$, $\Delta E_{\mathrm{BrHBr}} = 0.029$ eV) is illustrated in Figure 5(b). The similarity of the two wavefunction in the domain of the potential barrier, cf. Figures 5(a) and 5(b), and also the nearly perfect agreement of their mean energies (0.305 eV versus 0.307 eV) demonstrate convergence (11). Both wavefunctions are centered at the potential barrier, irrespective of the fact that some marginal fractions of the densities leak out essentially into a thin dumbbell-shaped layer—these leakages are negligible, for the present application, even though they may catch the eye because of their beautiful patterns. The layer may be interpreted as combination of two nearly spherical layers centered at the two bromine nuclei. These spheres

remind of the formation of the resonance BrHBr(vib = (00^00)) from reactants Br + HBr or HBr + Br, with rotationally excited diatomic molecules HBr($v = 0$). For comparison, Figure 5(c) illustrates the corresponding model wavefunction $\langle z, r, R|\psi_{\mathrm{BrHBr,pds},00^00}\rangle$ which is obtained as solution of Schrödinger Equation (12) with model PES (13)–(16) that serve as an approximation to the "true" PES, in the vicinity of its barrier; its parameters are derived from the peaks of the experimental pds and listed in the caption of Figure 9. We recall in passing that the parameter $V_{\mathrm{BrLBr,pdb,B}} = 0.300$ eV includes the ZPE of the symmetric stretch, $0.5\hbar\omega_{1,\mathrm{BrLBr}} = \sim 0.001$ eV—this estimate is deduced from the smallest spacing between the peaks in the high resolution spectra (not shown). As anticipated, this is entirely negligible compared to the barrier height, $V_{\mathrm{BrLBr,pdb,b}} = 0.300$ eV − 0.001 eV = 0.299 eV. Gratifyingly, this approximate value of the barrier height of the model potential agrees with the quantum chemical *ab initio* value $V_{\mathrm{BrLBr,b}} = 0.286$ eV,[10] within the theoretical and experimental values for the energy resolutions, $\Delta E_{\mathrm{BrHBr}} = 0.029$ eV and $\Delta E(v_3 = 0) = 0.025$ eV. Finally, Figure 5(d) illustrates the ground state wavefunction $\langle z, r, R|\psi_{\mathrm{BrHBr^-},00^00}\rangle$ of the precursor anion $BrHBr^-$. The resonance wavefunctions shown in Figures 5(a) and 5(b) are generated by putting this wavefunction in a FC-type manner from the bottom of the PES of $BrHBr^-$ to the PES of the neutral BrHBr and propagating it on V_{BrHBr}, cf. Eq. (10). This yields the apparent similarity of all the wavefunctions shown in Figures 5(a)–5(d), in the domain of the potential barrier. This similarity, together with the similar values of the mean energies 0.305 eV, 0.307 eV, and 0.327 eV, of the resonance wavefunctions shown in Figures 5(a)–5(c), respectively (with deviations below the experimental uncertainty $\Delta E(v_3 = 0)$), confirms the approximate validity of the model potential $V_{\mathrm{BrLBr,pds}}$.

Figure 6 documents corresponding 2D equidensity contours of the 3D resonance wavefunction $\langle z, r, R|\psi_{\mathrm{BrHBr},00^02}\rangle$ (Figure 6(a)) which correlates with the peak of the pds labeled $v_3 = 2$ in Figures 3(a) and 3(c). Figures 6(b) and 6(c) show the corresponding approximate resonance wavefunctions, which are entirely analogous to the approximations (Figures 5(b) and 5(c)) to the resonance wavefunction $\langle z, r, R|\psi_{\mathrm{BrHBr},00^00}\rangle$ (Figure 5(a)). Again, the similarity of these wavefunctions in the domain of the potential barrier and also the similar values of the accurate (Figure 6(a)) and approximate (Figures 6(b) and 6(c)) resonance energies demonstrate convergence (11) together with the approximate validity of model potential (13)–(16). The marginal leakage of the density of the resonance wavefunction from the domain of the barrier into the thin, dumbbell-shaped double layer with overall twin-spherical topology reminds of the formation of this resonance from rotationally and vibrationally ($v = 1$) excited reactants HBr + Br or Br + HBr.

Figures 7 and 8 illustrate the resonance wavefunctions $\langle z, r, R|\psi_{\mathrm{BrDBr},00^00}\rangle$ (Figure 7(a)) and $\langle z, r, R|\psi_{\mathrm{BrHBr^-},00^02}\rangle$ (Figure 8(a)) which belong to the peaks of the pds labeled $v_3 = 0$ and 2 which are documented in Figure 4 for the heavier isotopomer BrDBr. Also shown are the corresponding two approximations, cf. Figures 7(b) and 7(c) and Figures 8(b) and 8(c), and the wavefunction of the precursor anion $BrDBr^-(00^00)$, cf. Figure 7(d). The arrangement and analyses of Figures 7 and 8 for BrDBr are entirely analogous to Figures 5 and 6 for BrHBr. As provisional, very important result, Figures 3–8 support the approximate validity of model potential (13)–(16) for quantum simulations of the wavefunctions which are centered at the systems' potential barrier, together with their energies.

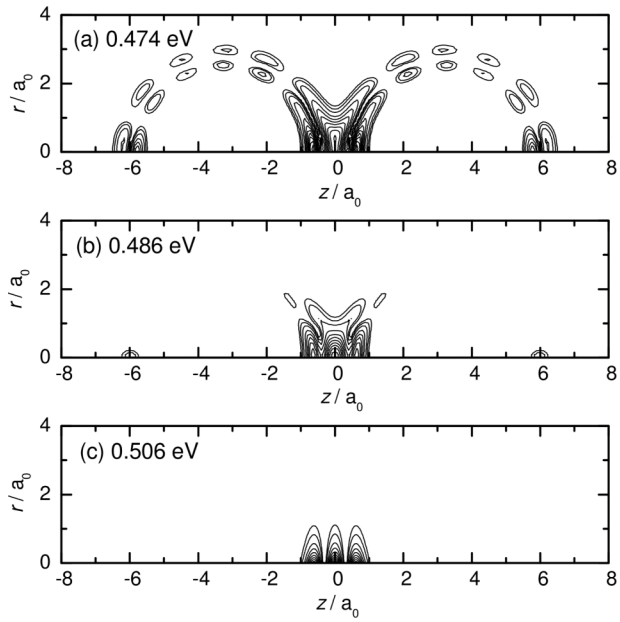

FIG. 6. Same as or analogous to Figure 5, panels (a)-(c), but for the second peak ($v_3 = 2$) of the pds shown in Figures 3(a) and 3(c).

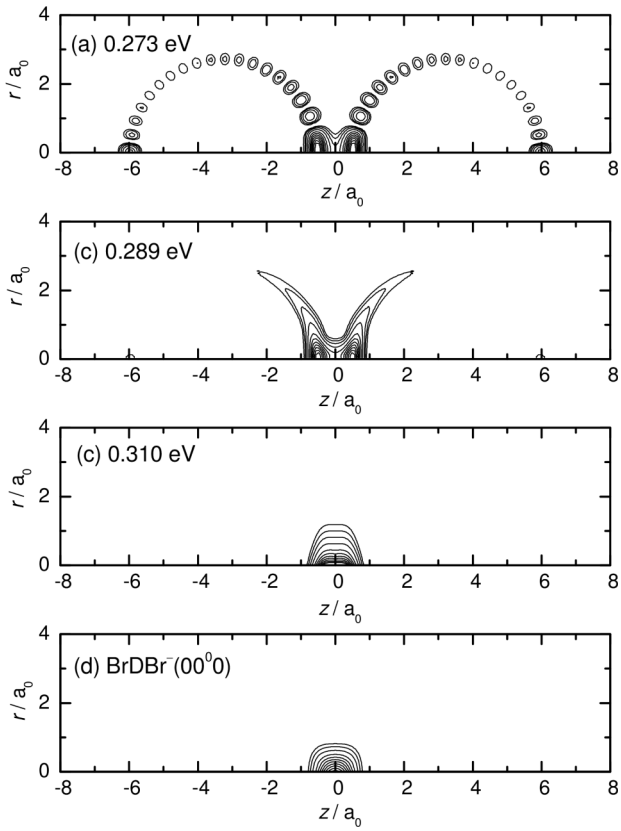

FIG. 7. Same as or analogous to Figure 5, but for BrDBr, compare with Figures 4(a) and 4(b).

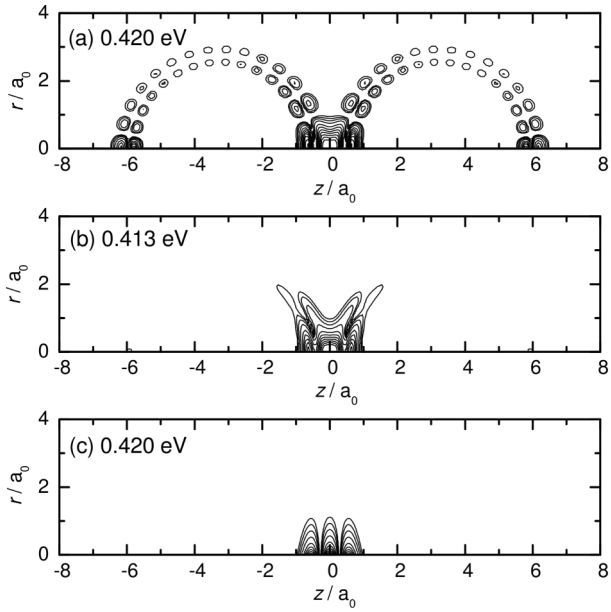

FIG. 8. Same as or analogous to Figure 6, but for BrDBr, compare with Figures 4(a) and 4(c).

Figures 9(a) and 9(b) illustrate 3D model potential (13)–(16) which has been deduced from the experimental pds,[1,2] together with the 3D model wavefunctions, by 1D profiles along z, Eq. (16). These 1D potentials $V_{z,\mathrm{BrLBr}}$ are shifted by the sum of the potential barrier $V_{\mathrm{BrLBr,pds,b}}$ plus the negligible ZPE $0.5\hbar\omega_{1,\mathrm{BrLBr}}$ of the symmetric stretch plus the significant ZPE of the doubly degenerate bend, $\hbar\omega_{2,\mathrm{BrLBr}}$, cf. Eq. (17). The parameters of the model potential are listed in the caption of Figure 9. Embedded in $V_{z,\mathrm{BrLBr}}$ are the vibrational levels $E_{\mathrm{BrLBr,pds},00^0v_3}$, v_3 = 0-4, Eq. (17), together with 1D profiles of the densities for the wavefunctions along the asymmetric stretch (v_3 = 0, 2, 4, only). The energies of the corresponding peaks labeled v_3 = 0, 2, 4 of the experimental pds are also given (in brackets) in Figures 9(a) and 9(b), compare with Figures 3 and 4 for the isotopomers BrHBr and BrDBr, respectively. Again, these energies are larger than the thresholds $E_{\mathrm{HBr},0}$ and $E_{\mathrm{DBr},0}$ [in square brackets], which means the vibrational states with the levels shown in Figures 9(a) and 9(b) are resonances with character of vibrational bonding, but not vibrationally bonded states.

In the last step towards our first goal, we now apply model potential (13)–(16) which has been deduced from the pds of $BrHBr^-$ and $BrDBr^-$, cf. Figures 9(a) and 9(b), to determine the corresponding approximate energy of BrMuBr(00^00). The result is $E_{\mathrm{BrMuBr,pds},00^00} = 0.461$ eV, see Figure 9(c). Apparently, this is below the threshold, $E_{\mathrm{MuBr},0} = 0.481$ eV. Its density is centered at the barrier of the PES. Accordingly, BrMuBr(00^00) is vibrationally bonded.

The present estimate $E_{\mathrm{BrMuBr,pds},00^00} = 0.461$ eV should be compared with the accurate quantum *ab initio* value 0.425 eV presented in Ref. 10. Apparently, the larger approximate value 0.461 eV is a conservative estimate; it may be considered as upper limit to the accurate level. By extrapolation, if the estimate $E_{\mathrm{XMuX,pds},00^00}$ is below the threshold $E_{\mathrm{LX},0}$, then the accurate value $E_{\mathrm{XMuX,pds},00^00}$ should be even lower below the threshold.

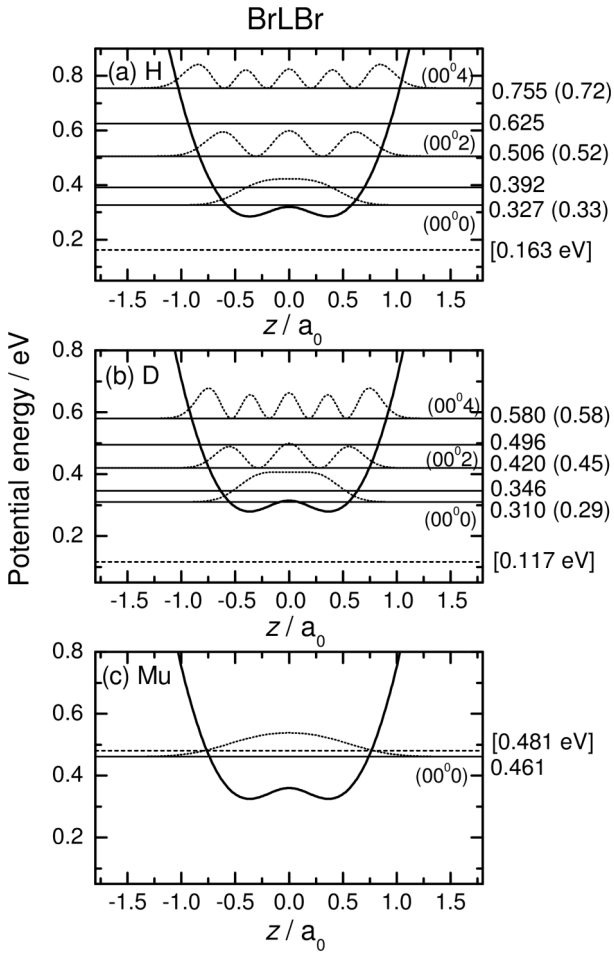

FIG. 9. The one-dimensional 1D profile $V_{z,\mathrm{BrLBr,pds}}$ of 3D model PES $V_{\mathrm{BrLBr,pds}}$ (13)–(16), together with the levels $E_{\mathrm{BrLBr,pds},00^0v_3}$ of the 3D vibrational resonances BrHBr(00^0v_3) (a) and BrDBr(00^0v_3) (b) or the vibrationally bonded BrMuBr(00^00) (c). The parameters of the 3D $V_{\mathrm{BrLBr,pds}}$ are $V_{\mathrm{BrLBr,B}} = 0.300$ eV, $f_{z,\mathrm{BrLBr}} = 2.75$ eV/a_0,[2] $z_{e,\mathrm{BrLBr}} = 0.500\,a_0$, $f_{r,\mathrm{BrLBr}} = 0.0272$ eV/a_0,[2] and $V_{\mathrm{lr,BrLBr}} = 0.220$ eV. These parameters are derived from the experimental pds of $BrHBr^-$ and $BrDBr^-$.[1,2] The 1D profile $V_{z,\mathrm{BrLBr}}$ of the 3D $V_{z,\mathrm{BrLBr}}$ has been shifted by the sum $V_{\mathrm{BrLBr,pds,B}} = V_{\mathrm{BrLBr,pds,b}} + 0.5\hbar\omega_{1,\mathrm{BrLBr}}$ of the parameter for the barrier height plus the negligible value 0.001 eV of the ZPE of the symmetric stretch (see text) plus the ZPE $\hbar\omega_{2,\mathrm{BrLBr}}$ of the doubly degenerate bend. The theoretical levels (without brackets) are compared with the values of the peaks of the pds labeled v_3, when available from Refs. 1 and 2. Also shown are the thresholds $E_{\mathrm{LBr},0}$, which means the vibrational ZPEs of the reactants LBr + Br or Br + LBr [in square brackets]. Levels $E_{\mathrm{BrLBr,pds},00^0v_3} < E_{\mathrm{LBr},0}$ belong to vibrationally bonded states, else they belong to vibrational resonances with character of vibrational bonding. The 3D energy levels embedded in the 1D profiles of the 3D PES also serve as baselines for 1D cuts of the 3D densities of the related wavefunctions.

At the end of this subsection, it is important to compare the bond energy 0.481 − 0.461 = 0.020 eV of the vibrationally bonded BrMuBr, as deduced from the pds of $BrHBr^-$ and $BrDBr^-$ (Figure 9(c)), with the accuracy of the empirical approach. Here, we have to consider two aspects. First, the comparison of the theoretical low and high resolution spectra (Figures 1 and 2) shows that the spectral peaks of the low resolution spectra may deviate from the levels of the reference states with optimal localization at the barrier (which means the states with "best character of vibrational bonding") by as much as ±0.017 eV. We assume the same deviation also between the peaks of the experimental spectra and the

reference states. Second, the theoretical levels for the 3D model potential deviate from the experimental spectral peaks by less than 0.03 eV. Considering both effects together, the theoretical levels for the model potential may deviate from the real reference states by as much as 0.047 eV. This is larger than the binding energy 0.02 eV of BrMuBr. Hence, we have to be careful and must say that the photoelectron detachment spectra of $BrHBr^-$ and $BrDBr^-$ allow to predict vibrational bonding of BrMuBr with bond energy 0.02 eV, but this suffers from the rather large uncertainty, i.e., ±0.047 eV. Gratifyingly, this empirical prediction has already been confirmed by the *ab initio* calculation in Ref. 10. The present investigation shows that the *ab initio* result for the bond energy 0.056 eV for the vibrationally bonded BrMuBr is uncertain within ±0.047 eV, which means it is "safe" compared with the empirical result.

B. From photoelectron detachment spectra of IHI^- and IDI^- to vibrational bonding of IMuI

The way from the pds of IHI^- and IDI^- to vibrational bonding of IMuI is documented in Figure 10, entirely analogous to Figure 9 for the way from the pds of $BrHBr^-$ and $BrDBr^-$ to vibrational bonding of BrMuBr. Specifically, the values of the experimental peaks of the pds labeled $v_3 = 0, 2, 4$ are obtained

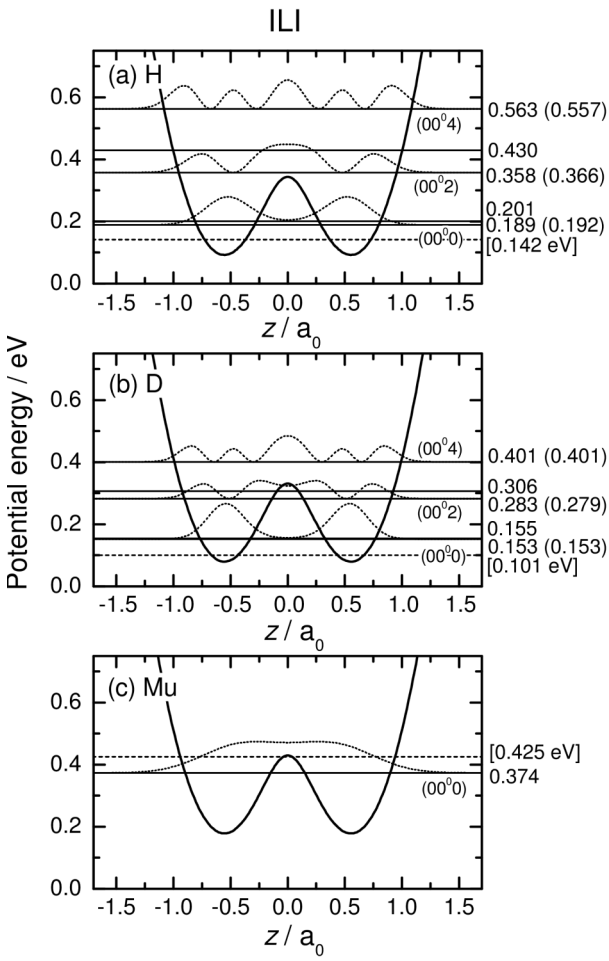

FIG. 10. Same as Figure 9, but for ILI. The parameters of 3D model PES $V_{\mathrm{ILI,pds}}$ Eqs. (13)–(16) are $V_{\mathrm{ILI,B}} = 0.300$ eV, $f_{\mathrm{z,ILI}} = 3.675$ eV/a_0,[2] $z_{\mathrm{e,ILI}} = 0.600\ a_0$, $f_{\mathrm{r,ILI}} = 0.0128$ eV/a_0,[2] and $V_{\mathrm{lr,ILI}} = 0.251$ eV.

from the experimental spectra documented in Refs. 2 and 11, using Eq. (6). For the energies on the right hand side of Eq. (6), we adapt the values $h\nu = 4.660$ eV,[2,11] $D_{\mathrm{IHI^-,0}} = 0.737$ eV,[22,33] $D_{\mathrm{IDI^-,0}} = 0.735$ eV,[22,33] $E_{I,\mathrm{a}} = 3.059$ eV,[31] $E_{\mathrm{HI,0}} = 0.142$ eV, and $E_{\mathrm{DI,0}} = 0.101$ eV.[32] The resulting experimental peak energies are given in Figures 10(a) and 10(b) (in brackets), together with the thresholds $E_{\mathrm{LI,0}}$ [in square brackets]; the values for $E_{\mathrm{HI,0}}$ and $E_{\mathrm{DI,0}}$ allow to extrapolate the threshold $E_{\mathrm{MuI,0}}$ by corresponding scalings of the zero point energies of a Morse potential for the diatomic molecules HI, DI, and MuI, respectively. From the experimental peaks of the pds labeled $v_3 = 0, 2, 4$, we then determine the model potential $V_{\mathrm{ILI,pds}}$ which serves as approximation to the "true" V_{ILI}, in the vicinity of the potential barrier. Again, $V_{\mathrm{ILI,pds}}$ takes the form of Eqs. (13)–(16); its parameters are determined such that the resulting energies $E_{\mathrm{ILI,pds},00^0v_3}$, $v_3 = 0, 2, 4$, Eq. (17), agree as well as possible with the corresponding experimental peak energies. The resulting optimal values of the parameters are listed in the caption of Figure 10. The symmetric 1D double well profiles of the resulting 3D model potential along z, shifted by the zero point energies for the symmetric stretch and the doubly degenerate bends, are shown in Figure 10, together with the levels $E_{\mathrm{ILI,pds},00^0v_3}$ and the 1D profiles of the densities of the related wavefunctions $\langle r, z, R|\psi_{\mathrm{ILI,pds},00^0v_3}\rangle$, analogous to Figure 9. Remarkably, the double well of the 1D profile of the 3D $V_{\mathrm{ILI,pds}}$ is significantly deeper than that for $V_{\mathrm{BrLBr,pds}}$, compare Figures 9 and 10. This trend is also reproduced by 1D cuts of the 3D *ab initio* potential V_{ILI} (see below) along z, compared to V_{BrLBr}, at the transition states. This may be rationalized by the fact that the distance between the two iodine nuclei at the linear transition state, $R_{\mathrm{ILI,b}} = 6.85\ a_0$, is larger than $R_{\mathrm{BrLBr,b}} = 6.16\ a_0$. As a consequence, for ILI, there is slightly "more space" which allows the central light atom L to relax to deeper values of the PES compared to BrLBr.

The comparison of the energies of IHI and IDI with vibrational quantum numbers 00^0v_3 for the model (without brackets) and the experimental peaks (with brackets) is documented in Figures 10(a) and 10(b). The overall agreement is of the same quality as in Figures 9(a) and 9(b) for BrHBr and BrDBr, respectively. By analogy, we conclude that the present model potential $V_{\mathrm{ILI,pds}}$ should allow reliable estimates of the energies of selective states of ILI which could be either vibrationally bound states or resonances with "character of vibrational bonding."

Clearly, all the vibrational levels shown in Figures 10(a) and 10(b) are above the thresholds $E_{\mathrm{HI,0}}$ and $E_{\mathrm{DI,0}}$, respectively. This means that the corresponding states are resonances. The 1D profiles of the densities of the wavefunctions show that the wavefunctions for $v_3 = 0$ and 2, 4 are centered close to, or at the potential barrier, i.e., they represent resonances with character of vibrational bonding. This confirms the conclusions of the experimentalists: IHI and IDI are not vibrationally bonded; instead, they are vdW bonded.[2,11]

In the last step, we employ the model potential $V_{\mathrm{ILI,pds}}$ which has been deduced from the pds of IHI^- and IDI^- in order to evaluate the approximate energy $E_{\mathrm{IMuI,pds},00^00}$ of IMuI in its vibrational state 00^00. The result is documented in Figure 10(c). Obviously, $E_{\mathrm{IMuI,pds},00^00}$ is below the threshold $E_{\mathrm{MuI,0}}$, which means it is a bound state. Moreover, the

1D profile of the density for the related wavefunction $\langle r, z, R|\psi_{\mathrm{IMuI,pds},00^00}\rangle$ along z shows that it is centered at the potential barrier. Hence, IMuI is a vibrationally bonded molecule.

The empirical results for vibrational bonding of IMuI, derived from the photodetachment spectra of IHI^- and IDI^-, call for confirmation by *ab initio* calculations. For this purpose, we have constructed a global potential energy surface of the I + HI reaction system. *Ab initio* electronic structure calculations were carried out at the MRCI + Q (multi-reference configuration interaction with Davidson correction) level of theory using the MOLPRO program.[34] The molecular orbital was calculated with the state-average CASSCF (complete-active-space self-consistent-field) wavefunction where 15 electrons were distributed among 9 orbitals. The augmented cc-pVQZ basis set[35] with additional diffuse functions was used for H while the effective-core SDB-aug-cc-pVTZ basis set[36] was used for I. The lowest seven electronic states were used in subsequent Breit-Pauli spin-orbit CI calculations to obtain the potential energy surfaces for the lowest three electronic states asymptotically correlating to $I(^2P_{3/2}$ and $^2P_{1/2}) + HI(X^1\Sigma)$. A total of about 24 000 *ab initio* energy points were generated and a cubic spline interpolation technique was used to obtain a global potential energy surface. The calculated potential energy surface has a barrier of 0.220 eV at the bent structure with each HI distance being 3.424 a_0 and the IHI angle being 161°. The barrier height at the linear transition state (second-order saddle point) structure is calculated to be 0.223 eV, indicating that the bending potential around the transition state is very flat. It is worth mentioning that the barrier height of the I + HI reaction is slightly lower than Br + HBr.[10] For the IHI^- anion, electronic structure calculations were performed at the coupled-cluster single double and perturbative triple excitation (CCSD(T)) level of theory with the same basis sets as used in the neutral system.

The resulting pds of IHI^- and IDI^- are compared with the experimental ones[2] in Figures 11 and 12, respectively, analogous to Figures 3 and 4 for $BrHBr^-$ and $BrDBr^-$. The overall agreement is satisfactory, with maximum deviations between the experimental and theoretical high resolutions peaks below 0.04 eV. The theoretical low resolution spectrum for IHI^- reproduces not only the dominant peaks which can be assigned to excitations of the asymmetric stretch with quantum numbers v_3 = 0, 2, 4 but also in the low energy range from ca. 0.2 to 0.35 eV; it also accounts for the progression of the experimental spectra which are due to a combination of bending motions and orbiting of the H atom around one or the other iodine nuclei. The detailed analysis of these resonance structures will be discussed in our future publication. In Figure 13, we also illustrate the resulting 3D wavefunction representing the vibrational bonded IMuI, by means of 2D equidensity contours. The corresponding 3D equidensity contours may be generated by rotating the 2D contours around the I-I internuclear (z-) axis. The resulting double cone type structure is similar to the shape of the density of the 3D wavefunction representing vibrationally bonded BrMuBr.[10] Moreover, the *ab initio* density of the vibrationally bonded IMuI is similar to the density for the wavefunction of IMuI supported by the empirical model potential which has been derived from the

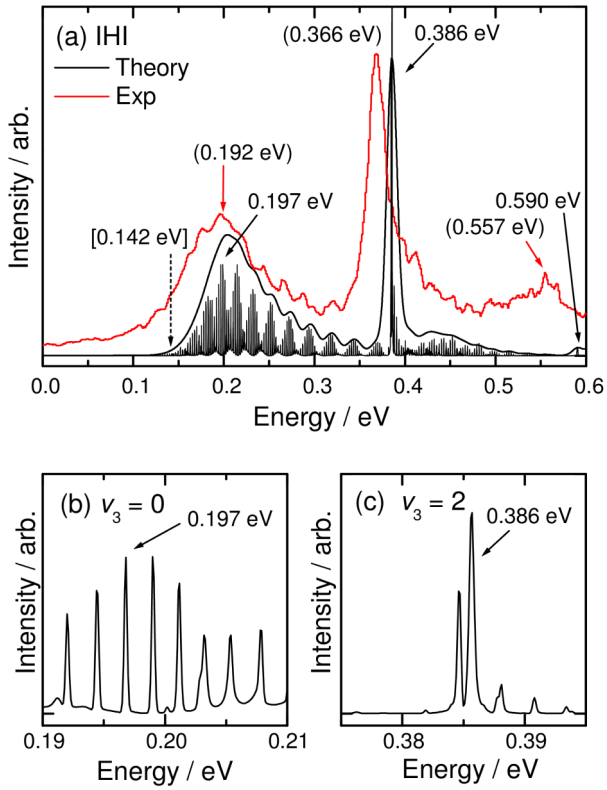

FIG. 11. Comparison of the experimental photoelectron photodetachment spectrum of IHI^- (adapted from Ref. 2) with the present theoretical low and high resolution spectra. The notations are analogous to those of Figure 3.

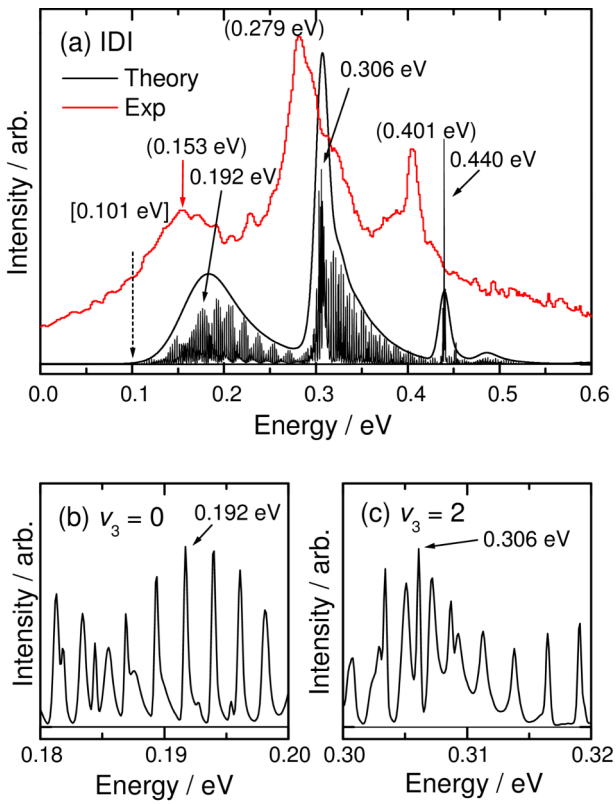

FIG. 12. Comparison of the experimental photoelectron photodetachment spectrum of IDI^- (adapted from Ref. 2) with the present theoretical low and high resolution spectra. The notations are analogous to those of Figures 3 and 4.

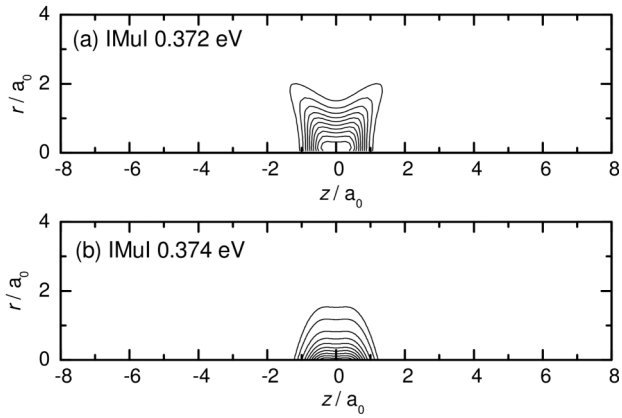

FIG. 13. 2D equidensity plot of the 3D wavefunction of vibrationally bonded IMuI: (a) *ab initio* result and (b) result for the 3D model potential.

experimental photodetachment spectra of IHI^- and IDI^-, compare Figures 13(a) and 13(b). The eigenenergies of IMuI for the *ab initio* and empirical potentials agree also well with each other. Most importantly, these *ab initio* and empirical energy levels for the ground state of IMuI are below the asymptotic threshold by more than 0.05 eV, compare with Figure 10(c). This energy gap is larger than the maximum uncertainty of the theoretical energies which has been assessed by comparison of the experimental and theoretical spectra, i.e., it is larger than 0.04 eV, cf. Figures 11 and 12. This confirms vibrational bonding of IMuI.

Finally, with the *ab initio* results for ILI at hand, it is also instructive to assess the uncertainty of the empirical prediction of vibrational bonding of IMuI, with bond energy 0.425 – 0.374 = 0.051 eV (Figure 10(c)), deduced for the pds for IHI^- and IDI^-. Considerations of the deviations between the peaks of the theoretical high and low resolution spectra and between the experimental and theoretical peaks of the pds for IHI^- and IDI^-, analogous to those made for $BrHBr^-$ and $BrDBr^-$, yield the uncertainty ±(0.010 + 0.039 = 0.049) eV, slightly smaller than the predicted bond energy.

IV. CONCLUSIONS

We have developed a method which allows to use experimental photoelectron detachment spectra of dihalogen hydride anions XHX^- and XDX^-, in order to predict vibrational bonding of XMuX. The method profits from the favorable property of these radicals, which enables transition state spectroscopy of the neutrals XHX and XDX, namely, the near coincidence of the geometric structures of XLX^- at the potential minimum $V_{XLX^-,m}$ and XLX at the potential barrier $V_{XLX,b}$. The present results confirm the previous experimental results,[1–3,11] namely, neither BrHBr, BrDBr nor IHI, IDI are vibrationally bonded; nevertheless, BrHBr, BrDBr and IHI, IDI support vibrational resonances with "character of vibrational bonding," i.e., the corresponding wavefunctions are centered at the potential barrier. In contrast, both BrMuBr and IMuI are predicted to be vibrationally bonded molecules. In the case of BrMuBr, this confirms the result of Ref. 10, which is based on highly accurate quantum chemistry *ab initio* calculations of the molecule's potential energy surface. Here, the same result is derived from the experimental pds, without any *ab initio* calculations, see Figure 9. The latter have been used, however, to illustrate and support the general approach, cf. Figures 3–8. In the case of ILI, we could employ this empirical approach in order to predict vibrational bonding of IMuI, based on the experimental pds of IHI^- and IDI^-, see Figure 10.[2,11] Figure 10 thus establishes IMuI as second example of a molecule which is bound by vibrational bonding, analogous to Figure 9 which confirms BrMuBr as the first example.[10] At the same time, Figures 9 and 10 confirm the previous experimental results,[1–3,11] i.e., neither BrHBr, BrDBr nor IHI, IDI are vibrationally bonded, instead they are vdW bonded. As a summary, Figure 9 confirms the recent discovery of the fundamental change of the nature of chemical bonding, from vdW bonding of BrDBr, BrHBr to vibrational bonding of BrMuBr. Figure 10 extends this isotope effect to the second example of isotopomers IDI, IHI, and IMuI.

The empirical results for vibrational bonding of IMuI derived from the pds of IHI^- and IDI^- have been confirmed by *ab initio* simulations. On the way, we carried out *ab initio* simulations of the pds of IHI^- and IDI^-, with high (state-resolved) and low resolutions (similar to the experimental one). Likewise, we have simulated the pds of $BrHBr^-$ and $BrDBr^-$. Comparisons of selected prominent peaks of the theoretical high and low resolution spectra, as well as the theoretical and experimental low resolution spectra, allowed an assessment of the accuracy of the empirical and the *ab initio* predictions of vibrational bonding of BrMuBr and IMuI. Accordingly, the empirical value of the bond energy of IMuI is slightly larger than its uncertainty, which means the pdb of IHI^- and IDI^- allow the firm prediction of vibrational bonding of IMuI. The pds for $BrHBr^-$, $BrDBr^-$ also allow to predict vibrational bonding of BrMuBr, but this prediction suffers from uncertainties which exceed the predicted bond energies. Ultimately, the empirical deductions of vibrational bonding of both BrMuBr and IMuI from the pds spectra of $BrHBr^-$, $BrDBr^-$ and IHI^-, IDI^- are confirmed by *ab initio* calculations with uncertainties ±0.046 eV and ±0.039 eV which are smaller than the bond energy 0.056 eV and 0.053 eV, respectively.

ACKNOWLEDGMENTS

We would like to express sincere thanks to Professor D. G. Fleming (TRIUMF, Vancouver) for stimulating discussions.

[1]R. B. Metz, A. Weaver, S. E. Bradforth, T. N. Kitsopoulos, and D. M. Neumark, J. Phys. Chem. **94**, 1377 (1990).
[2]R. B. Metz, S. E. Bradforth, and D. M. Neumark, Adv. Chem. Phys. **81**, 1 (1992).
[3]H. Gómez, G. Meloni, J. Madrid, and D. M. Neumark, J. Chem. Phys. **119**, 872 (2003).
[4]S. Baer, D. Fleming, D. Arseneau, M. Senba, and A. Gonzalez, *Isotope Effects in Chemical Reactions and Photodissociation Processes*, American Chemical Society Symposium Series Vol. 502, edited by F. A. Kaye, (Washington, DC, 1992), pp. 111–137.
[5]D. G. Fleming and M. Senba, in *Perspectives in Meson Science*, edited by T. Yamazaki, K. Nakai, and K. Nagamine (North Holland, Amsterdam, 1992), pp. 219–260.
[6]M. Lorenz, D. Kraus, M. Räsänen, and V. E. Bondybey, J. Chem. Phys. **112**, 3803 (2000).
[7]S. C. Kettwich, L. F. Pinelo, and D. T. Anderson, Phys. Chem. Chem. Phys. **10**, 5564 (2008).

[8]T. Takayanagi, Chem. Phys. **334**, 109 (2007).
[9]R. Toboła, G. Chałasiński, J. Kłos, and M. M. Szczęśniak, J. Chem. Phys. **130**, 184304 (2009).
[10]D. G. Fleming, J. Manz, K. Sato, and T. Takayanagi, Angew. Chem., Int. Ed. **53**, 13706 (2014).
[11]A. Weaver, R. B. Metz, S. E. Bradforth, and D. M. Neumark, J. Phys. Chem. **92**, 5558 (1988).
[12]J. Manz, R. Meyer, E. Pollak, and J. Römelt, Chem. Phys. Lett. **93**, 184 (1982).
[13]D. C. Clary and J. N. L. Connor, Chem. Phys. Lett. **94**, 81 (1983).
[14]J. Manz, R. Meyer, and J. Römelt, Chem. Phys. Lett. **96**, 607 (1983).
[15]J. Manz, R. Meyer, E. Pollak, J. Römelt, and H. H. R. Schor, Chem. Phys. **83**, 333 (1984).
[16]D. C. Clary and J. N. L. Connor, J. Phys. Chem. **88**, 2758 (1984).
[17]J. Manz, R. Meyer, and H. H. R. Schor, J. Chem. Phys. **80**, 1562 (1984).
[18]G. C. Schatz, J. Phys. Chem. **94**, 6157 (1990).
[19]C. Kubach, G. Nguyen Vien, and M. Richard-Viard, J. Chem. Phys. **94**, 1929 (1991).
[20]E. Pollak, in *Jerusalem Symposium on Quantum Chemistry and Biochemistry: Intramolecular Dynamics*, edited by B. Pullman and J. Jortner (Reidel, Dordrecht, 1982), pp. 1–16.
[21]E. Pollak, Chem. Phys. Lett. **94**, 85 (1983).
[22]R. B. Metz and D. M. Neumark, J. Chem. Phys. **97**, 962 (1992).
[23]C. L. Russell and D. E. Manolopoulos, Chem. Phys. Lett. **256**, 465 (1996).
[24]J. H. Frederick and E. J. Heller, J. Chem. Phys. **87**, 6592 (1987).
[25]R. Schinke, *Photodissociation Dynamics* (Cambridge University Press, Cambridge, 1995), pp. 160–163.
[26]M. R. Wall and D. Neuhauser, J. Chem. Phys. **102**, 8011 (1995).
[27]I. Barth, J. Manz, G. Pérez-Hernández, and P. Sebald, Z. Phys. Chem. **222**, 1311 (2008).
[28]M. D. Feit, J. A. Fleck, Jr., and A. Steiger, J. Comput. Phys. **47**, 412 (1982).
[29]K. Bergmann, S. Görtler, J. Manz, and H. Quast, J. Am. Chem. Soc. **115**, 1490 (1993).
[30]D. L. Carroll, AIAA J. **34**, 338 (1996).
[31]H. Hotop and W. C. Lineberger, J. Phys. Chem. Ref. Data **14**, 731 (1985).
[32]See http://webbook.nist.gov/chemistry/ for National Institute of Standards and Technology, NIST Chemistry WebBook.
[33]G. Caldwell and P. Kebarle, Can. J. Chem. **63**, 1399 (1985).
[34]H.-J. Werner, P. J. Knowles, G. Knizia, F. R. Manby, M. Schütz *et al.*, MOLPRO, version 2010.1, a package of *ab initio* programs, 2010, see http://www.molpro.net.
[35]T. H. Dunning, Jr., J. Chem. Phys. **90**, 1007 (1989).
[36]J. M. L. Martin and A. Sundermann, J. Chem. Phys. **114**, 3408 (2001).